

Tornado-Producing Mini Supercells Associated with Typhoon 9019

OSAMU SUZUKI

Japan Meteorological Agency, Ohtemachi, Chiyoda, Tokyo, Japan

HIROSHI NIINO

Ocean Research Institute, University of Tokyo, Minamidai, Nakano, Tokyo, Japan

HISAO OHNO

Meteorological College, Asahi-cho, Kashiwa, Chiba, Japan

HIROSHI NIRASAWA

Japan Meteorological Agency, Ohtemachi, Chiyoda, Tokyo, Japan

(Manuscript received 3 August 1998, in final form 11 June 1999)

ABSTRACT

On the night of 19 September 1990, nine mini-supercell storms were observed over the Kanto Plain of Japan in the northeast quadrant of Typhoon 9019. Three storms out of nine spawned a tornado. The characteristics of the storms and tornadoes were studied by means of a single Doppler radar, conventional radars, surface meteorological observations, and damage surveys.

The mini-supercell storms exhibited characteristics similar to typical supercell storms over the Great Plains of the United States, such as hook echo, bounded weak echo region, slower movement relative to the mean wind, long lives, and rightward deviation of the storm motion relative to the mean wind shear was observed. They also displayed several differences from typical supercell storms with respect to the following points: 1) horizontal scale of the mesocyclone was smaller; and 2) vertical vorticity was confined to lower levels (less than 5 km above ground level). These similarities and differences correspond with those observed for miniature supercells in Hurricane Danny's environment.

The storm environment for these mini supercells was characterized by modest convective available potential energy (about 1600 J kg^{-1}) and strong low-level wind shear with veering. The storm updrafts likely tilted the ambient horizontal vorticity associated with the strong low-level wind shear to generate mesocyclonic vertical vorticity.

Two of the tornadoes were spawned by mini-supercell storms moving along a preexisting surface boundary that was accompanied by significant convergence, vertical vorticity, and horizontal gradients of temperature. An estimation of vertical vorticity near the ground in the boundary suggests a possibility that preexisting vertical vorticity contributed to supercell evolution resulting in tornadogenesis.

1. Introduction

A significant number of tornadoes are known to occur in association with tropical cyclones such as hurricanes and typhoons. About 40% of the typhoons making landfall in the islands of Japan during 1961–82 produced at least one tornado (Mitsuta 1983) as did approximately 59% of the hurricanes that hit the United States during the period of 1948–86 (McCaul 1991).

Statistical studies on tropical cyclone-associated tornadoes have been made by many researchers (e.g., Fujita et al. 1972; Novlan and Gray 1974; Omoto 1982; Mitsuta 1983; McCaul 1991). These studies revealed that the prevalence for tornadic events in the northeast quadrant of a hurricane or typhoon (Novlan and Gray 1974; Gentry 1983) and that low-level vertical wind shear is a crucial factor for the occurrence of a tornado. Average vertical wind shear in the environments of tornadic storms as defined by the wind speed difference between the surface and 850 hPa was greater than 23 m s^{-1} for typhoon-associated tornadoes (Mitsuta 1983), and was greater than 20 m s^{-1} for hurricane-associated tornadoes (Novlan and Gray 1974). McCaul (1991) has demonstrated that the wind hodographs for the four storm

Corresponding author address: Dr. Osamu Suzuki, Japan Meteorological Agency, 1-3-4 Ohtemachi, Chiyoda, Tokyo 100-8122, Japan.
E-mail: osuzuki@mri-jma.go.jp

quadrants with respect to the hurricane motion vary significantly and that the right forward quadrant is the most preferred location for supercells and therefore for tornadoes. He speculated that helicity enhancement caused by the interaction of the hurricane's swirling flow with a steering current containing shear roughly parallel to the hurricane heading is responsible for the prevalence of hurricane-associated tornadoes in the hurricane's right-forward quadrant.

A surprisingly limited number of studies on the characteristics of parent storms of tropical cyclone-associated tornadoes have been performed. Most previous studies utilized data from surface observations and conventional radars. These studies suggest that parent storms of tropical cyclone-associated tornadoes are often supercells (e.g., Fujita et al. 1972; Omoto 1982; McCaul 1987). Fujita et al. (1972) analyzed the Ohmiya tornado associated with Typhoon 7113 in 1971, and found a mesocyclone in the parent storm. Omoto (1982) found that the parent storm of the Nagoya tornado associated with Typhoon 7912 in 1979 had characteristics similar to those of typical supercell storms over the Great Plains. However, the parent storm displayed little deviation to the right of the mean wind. Saito (1992) analyzed tornadoes associated with Typhoon 8019 in 1980 in Miyazaki prefecture and found that the tornadoes were accompanied by mesocyclones in the parent storms.

McCaul (1987) studied the parent storms of tornadoes associated with hurricane Danny in 1985. He found that the morphology of the parent storms, such as a hook-shaped echo, was similar to that of typical supercells over the Great Plains, though their scales both vertical and horizontal were smaller. Furthermore he found that the rightward or leftward deviation of the storm motion, which is often observed in typical supercells (e.g., Charba and Sasaki 1971) and for simulated supercells (e.g., Weisman and Klemp 1984), was less significant. It should be noted that not all the supercells deviate. McCaul also compared the environment of tornado-producing storms under hurricane Danny with that of typical supercell storms over the Great Plains. He pointed out that in the hurricane environment, vertical wind shear was stronger below a few kilometers above ground level (AGL) and was weaker above, and convective available potential energy (CAPE) was modest. Using a numerical simulation model, McCaul (1993) and McCaul and Weisman (1996) illustrated that storms similar to typical supercells, but with smaller horizontal and vertical scales, can be generated in the hurricane environment.

Doppler radar observations of tornadic storms in the hurricane or typhoon environment began only recently. Snell and McCaul (1993) succeeded in Doppler radar observation of tornado-producing storms in hurricane Andrew in 1992, detecting mesocyclones in the storms. They identified at least nine separate mesocyclones in Doppler radar data. The mesocyclones exhibited several

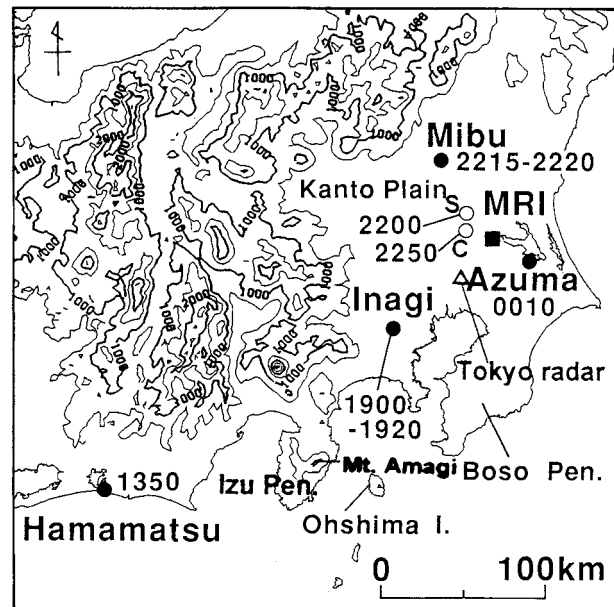


FIG. 1. Times and locations of tornadoes at Inagi city, Mibu town, and Azuma village and wind damages at Chiyokawa village (C in the figure) and Shimotsuma city (S). The locations of tornadoes and wind damages are indicated by solid and open circles, respectively, together with the times of occurrence in Japan Standard Time (JST). The location of MRI Doppler radar is indicated by the solid square and that of Tokyo is shown by the open triangle. Topography around the Kanto Plain is shown by the height contours drawn for every 500 m.

features similar to those observed in typical supercell storms. However, their circulation was smaller in horizontal scale, confined to below 4.7 km AGL. These characteristics were consistent with the results of numerical simulations made by McCaul (1993) and McCaul and Weisman (1996).

Similar small-scale supercells, labeled miniature supercells or mini supercells are reportedly associated with not only tropical cyclones but also extratropical cyclones (e.g., Burgess et al. 1995). Most mini supercells have been found in environments characterized by low strong vertical wind shear as found under a tropical cyclone (e.g., McCaul 1987) or an extratropical cyclone (Davies 1993; Guerrero and Read 1993). Burgess et al. (1995) examined mesocyclones detected by WSR-88D in 18 mini supercells and compared them with the traditional Oklahoma mesocyclones studied in Burgess et al. (1982). The comparison revealed similarities, such as in storm morphology and evolution, and differences, such as in mesocyclone scale. An averaged mesocyclone diameter and vertical extent for mini supercells are, respectively, as two-thirds and half of those of traditional Great Plains supercells.

On the night of 19 September 1990, three tornadoes occurred in the Kanto Plain in association with Typhoon 9019 (T9019). The locations and the times of the tornadoes are shown in Fig. 1, together with the topography around the Kanto Plain. The parent storms of these tor-

nadoes were observed by a Doppler radar at the Meteorological Research Institute (MRI) in Tsukuba, about 60 km northeast of Tokyo (see Fig. 1). In this paper, we will describe the characteristics of the tornadoes and their parent storms as revealed from damage surveys, surface meteorological data, conventional radars, and the Doppler radar.

In the following section, the data used for the present analysis are described. The synoptic condition that led to the mini-supercell formation and tornadogenesis are illustrated in section 3. The storm environment and surface boundary are examined in section 4. The characteristics of the tornadoes and parent storms are presented in section 5. Results are discussed in section 6, and summary and conclusions are given in section 7.

2. Data

In this section, the data used for the present analysis are described briefly. Detailed description of the data may be found in Niino et al. (1993).

Surface meteorological data were collected from local observatories and AMeDAS stations of the Japan Meteorological Agency (JMA), and environmental monitoring stations (EMS) of local governments. Figure 2 shows the locations and category of the stations. The AMeDAS stations are distributed one per $17 \text{ km} \times 17 \text{ km}$ square all over Japan on average. Most of the AMeDAS stations measure wind speed and direction, temperature, insolation, and precipitation every 10 min. The EMS are distributed with much higher density as seen in Fig. 2. A considerable fraction of the EMS measure only wind speed and direction.

A C-band¹ Doppler radar at MRI and two C-band conventional radars at Kashiwa (Tokyo radar) and Haneda were used for analysis. The Nyquist interval of the Doppler radar was $\pm 16 \text{ m s}^{-1}$. The MRI Doppler radar started its operation at 1918 JST² 19 September. Both Doppler velocity and reflectivity data were collected at 11 elevations every 12 min (full circle scans during 1918–2003 and 2200–0600 JST) or every 5 min (sector scans over western semicircle during 2008–2145 JST). Spatial resolutions are 500 m (1918–2145 and after 0005 JST) or 250 m (2149–2359 JST) in the radial and 1.4° in the azimuth. The two conventional radars provide precipitation intensity $R \text{ mm h}^{-1}$ calculated from the $Z-R$ relation of $Z = 200R^{1.6}$. Tokyo radar provides constant altitude plan position indicator (CAPPI) data at approximately 2 km AGL, while Haneda radar provides

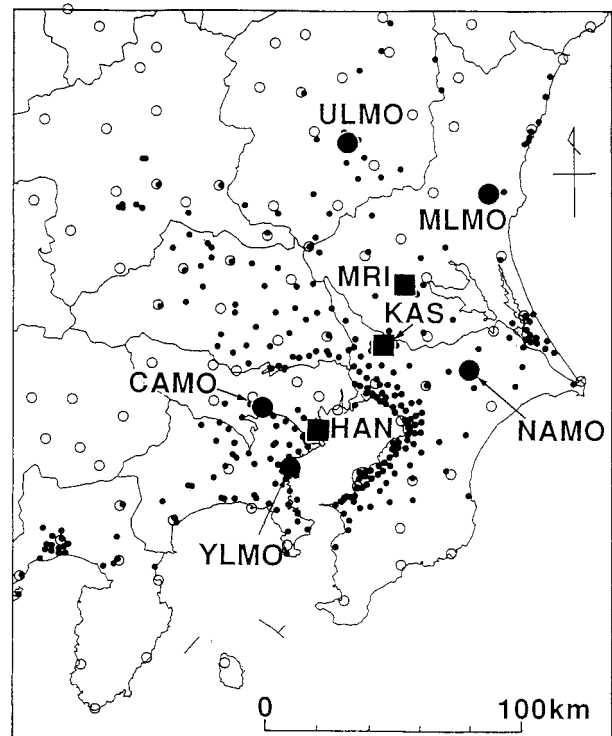


FIG. 2. Locations of surface meteorological stations and weather radars in the Kanto Plain. The closed circles show observatories of JMA. The open circles show AMeDAS stations of JMA. The dots show environmental meteorological stations of local governments. The solid squares show Doppler radar at MRI in Tsukuba and conventional radars at Kashiwa (Tokyo radar) and Haneda. Tateno, the upper-air sounding station, is only 500 m north of MRI, and is indistinguishable from the location of MRI in this scale.

plan position indicator (PPI) data with a constant elevation angle of 1.5° .

Upper-air soundings of wind, temperature, and humidity were available from Tateno Upper Air Observatory, which is located about 500 m north of the MRI Doppler radar site. The sounding interval was 6 h from 0900 JST 19 September to 0900 JST 20 September.

3. Synoptic conditions

Figure 3 shows the track of T9019 from 18 to 20 September, superimposed on an infrared image taken at 2100 JST by the Japanese Geostationary Meteorological Satellite (GMS-4). Typhoon 9019 moved northeastward and struck on the shoreline near Shirahama (33.6°N , 135.8°E) in Wakayama prefecture at around 2000 JST 19 September. At the time of landing, the typhoon's maximum wind speed and central surface pressure were 45 m s^{-1} and 945 hPa, respectively. Past statistical studies by Novlan and Gray (1974), Mitsuta (1983), and McCaul (1991) pointed out that the intensity of a tropical cyclone is an important factor for the ability to produce tornadoes. According to McCaul (1991), mean intensities of 21.9, 28.7, and 47.1 m s^{-1} were found for

¹ Wavelengths of the three C-band radars are approximately 5.7 cm.

² JST indicates Japan Standard Time. Hereafter, reference to time will be in JST; 0900 JST is 0000 UTC.

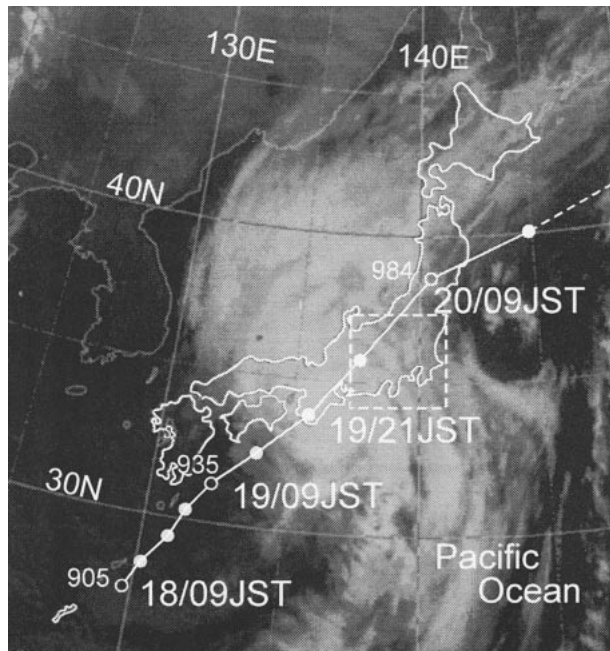


FIG. 3. Track of Typhoon 9019 from 18 to 20 Sep together with the satellite imagery taken by GMS-4 at 2100 JST 19 Sep. Typhoon 9019 landed at Shirahama in Wakayama prefecture in Honshu Island about 20 JST. Typhoon position is indicated by white solid and open circles at 0900 and 2100 JST, respectively. The number by each open circle shows the day. The Kanto Plain was in the northeast quadrant of the typhoon on the evening of 19 Sep. The box, drawn by dashed line, in the figure indicates the area of Fig. 1.

hurricanes that produced no tornado, one tornado, and more than eight tornadoes, respectively. The fact that T9019's intensity was 45 m s^{-1} at the landing produced four tornadoes consistent with his result. T9019 continued to move northeastward across the Honshu Island (the largest island of Japan), and reached the Pacific Ocean by 1100 JST 20 September. At the time of the satellite imagery, the typhoon was located about 500 km east-northeast of the Kanto Plain and southeasterly wind was prevailing in the plain.

The first of the four tornadoes associated with T9019 occurred in Hamamatsu in Shizuoka prefecture at 1350 JST, under an outer rainband of the typhoon. The rainband moved northward from the Pacific Ocean to Shizuoka prefecture and covered the Chubu district (central part of the Honshu Island) of Japan. Fig. 4 shows the hourly reflectivity fields by the Tokyo radar from 1600 to 2400 JST. Before 1730 JST, only scattered thunderstorms were found over the Kanto Plain (Figs. 4a,b). The rainband reached the Kanto Plain around 1730 JST, and eventually covered the western half of the Kanto Plain (Fig. 4c). This rainband seemed to be trapped by the orography of the Izu Peninsula and the western Kanto Plain. Most of the new cells in the cluster were generated near the northern side of Izu Peninsula, and propagated north-northeastward to form a bandlike echo in a line from Izu Peninsula to the northern Kanto Plain

(see Figs. 4d–f). This bandlike structure (seen as a yellow region in the figure) persisted during the period of 1800–2100 JST (Figs. 4c–f). Such a precipitation band is known to occur frequently when a warm moist southerly wind prevails over the Kanto Plain (e.g., Sekiguchi et al. 1964; Asai and Takahashi 1981). Asai and Takahashi (1981) analyzed a strong bandlike echo, which produced three tornadoes on 9 September 1976, and suggested that the Amagi Mountain in the Izu Peninsula was responsible for forming such bandlike echo. The vertical wind profile of the day displayed south-southeasterly winds veering slightly between 850 hPa and 700 hPa to nearly due south. Wind speed increased with height from several meters per second to about 18 m s^{-1} . These conditions were almost identical to those of 19 September 1990.

On the other hand, in the eastern half of the Kanto Plain, only scattered thunderstorms, sometimes accompanied by light to moderate rain associated with anvils of the thunderstorms, appeared occasionally and moved north-northeastward (Figs. 4d–i). The contrast in the echo pattern between the western and eastern Kanto Plain persisted until 0200 JST 20 September.

4. Storm environment

a. Vertical structure

Figure 5 presents upper sounding data gathered from 2030 to 2202 JST 19 September at Tateno. Since synoptic conditions changed very little and no significant storm nor frontal system passed over Tateno during the observation, the sounding is considered to give a good representation of the environment in which the storms developed on the eastern Kanto Plain.

The Showalter's stability index (SSI) value calculated from the sounding was about -2 K indicating an unstable environment. CAPE was about 1600 J kg^{-1} , and is comparable to that of the miniature supercell environment (1834 J kg^{-1}) under hurricane Danny in 1985 (McCaul and Weisman 1996). Though this value is significantly larger than the average CAPE value of the hurricane-tornado environment (e.g., 253 J kg^{-1} ; McCaul 1987), it is smaller than that of typical supercell environments over the Great Plains (e.g., 2542 J kg^{-1} for Oklahoma supercells; Bluestein and Jain 1985).

Figure 6 shows the wind hodograph obtained from the same sounding. Strong vertical shear with veering existed below 3 km AGL, which again is similar to that of hurricane Danny's case, indicated in the same figure by dashed line. The bulk Richardson number (BRN), introduced by Weisman and Klemp (1982), was 10, and is in the lower end of possible range for simulated and observed supercell storm development. Storm relative helicity (SRH), which is suggested to be an important component in quantitative measurements of the storm environment (e.g., Davies-Jones et al. 1990), was $310 \text{ m}^2 \text{ s}^{-2}$ assuming storm motion of 17 m s^{-1} to the north-

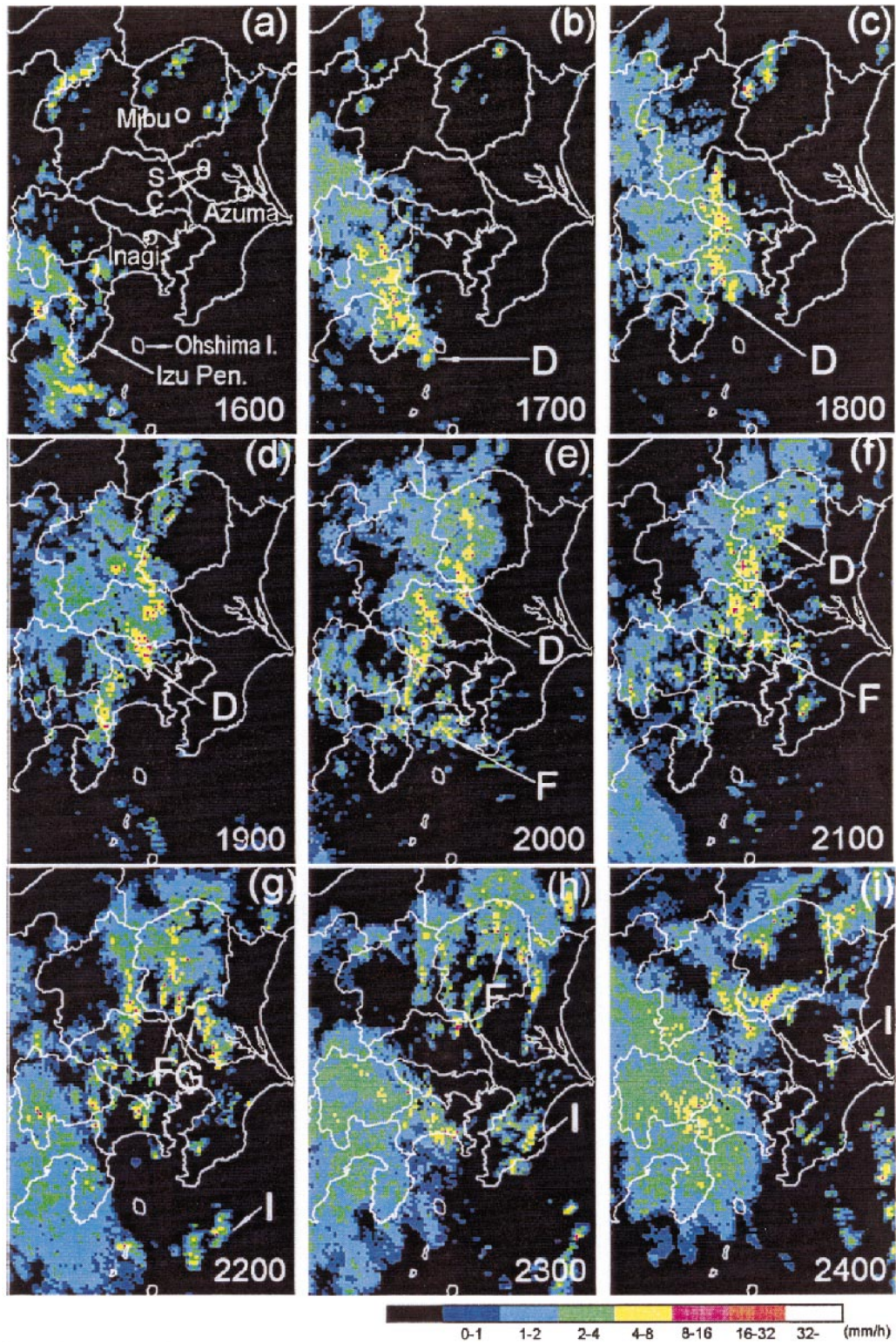


FIG. 4. Hourly PPI radar reflectivity map derived from Tokyo radar between 1600 and 2400 JST 19 Sep. Precipitation intensities are indicated by color bar. Locations of tornadoes, wind damages, Izu Peninsula, and Ohshima Island are indicated in the first panel. Alphabets in the figures with arrows show the mini-supercell storms identified by Doppler radar.

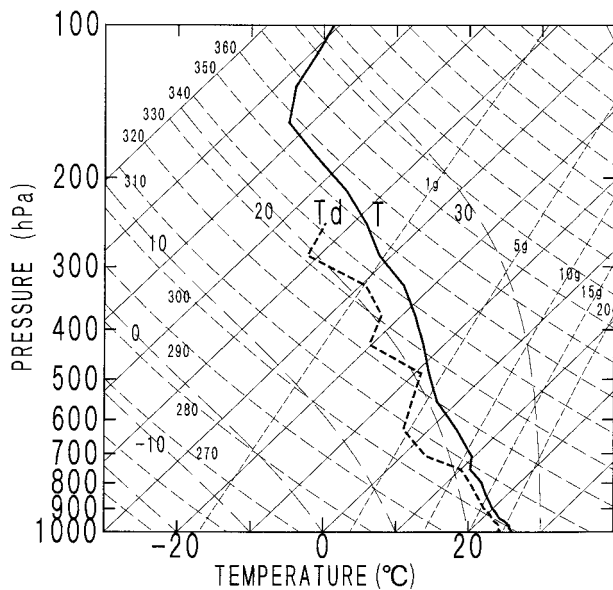


FIG. 5. Skew T -log p diagram of temperature and dewpoint temperature at Tateno at 2100 JST 19 Sep. CAPE is about 1600 J kg^{-1} .

northeast. This value is about twice that of the threshold value ($150 \text{ m}^2 \text{ s}^{-2}$) for mesocyclone formation noted by Davies-Jones et al. (1990). Although recent research (e.g., Davies-Jones 1993; Markowski et al. 1998) suggests that significant spatial and temporal variabilities may exist, the estimated CAPE, BRN, and SRH values indicate that the environment would support the development of supercells.

b. Preexisting surface boundary

When the prevailing wind is southerly, a mesoscale surface boundary often forms on the Kanto Plain, which is bordered from west to north by mountains ~ 1000 – 2000 m in height (e.g., Kawamura 1970). The boundary on such an occasion runs from north-northeast to south-southwest, and divides warm air in the southeast and cool stagnant air in the northwest. On the evening of 19 September, such a surface boundary with sharp temperature-gradient and wind shear did exist near the eastern edge of the precipitation region (see Fig. 4) over the western portion of the Kanto Plain.

Figure 7 shows the distribution of surface wind and temperature derived from AMeDAS and EMS at 1900 JST, together with the reflectivity map obtained by the Tokyo radar. The boundary is distinguishable, extending north-northeastward from the northeastern edge of the Izu Peninsula and located in the central Kanto Plain (see Fig. 1). The western side of the boundary contained cool air produced by the precipitation over the western Kanto Plain, and in the east side was warm air advected from south. The boundary had an eastward protuberance near the Inagi City where a tornado occurred between 1900 and 1920 JST. This protuberance may have been

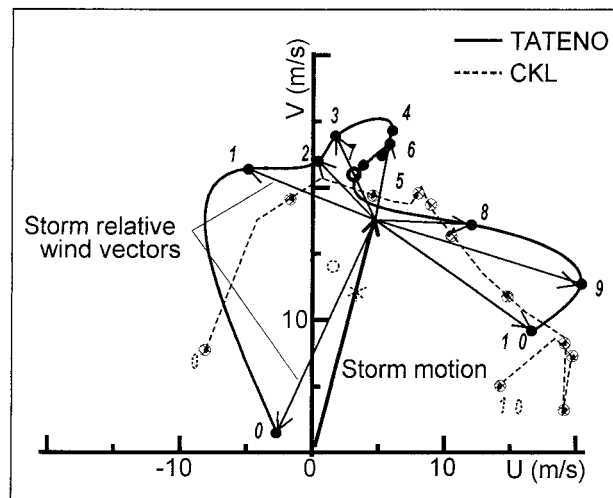


FIG. 6. Wind hodograph observed at Tateno at 2100 JST 19 Sep. The movement of storm F is indicated by the thick arrow, and the density-weighted mean wind below 10 km AGL by the open circle. Numbers by the solid circles on the curve indicate height in kilometers and 0 the surface. The thin arrows shows storm relative winds at each height. Dashed line and dashed letters indicate wind hodograph and heights at Centreville, Alabama (CKL), 0000 UTC 17 Aug 1985 (McCaul 1987).

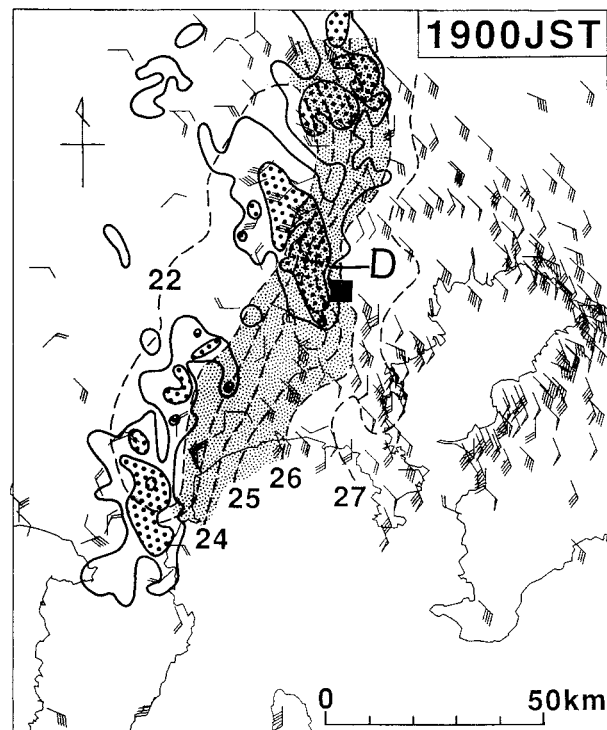


FIG. 7. Distribution of surface temperature and winds derived from surface meteorological stations at 1900 JST 19 Sep. Dashed lines denote temperature contours drawn for each 1 K. Wind barb and flag represent 1 m s^{-1} and 5 m s^{-1} , respectively. Contour lines of radar reflectivity are also shown for each 10 dB by solid lines. Areas where reflectivity is greater than 30 dBZ are hatched. The shaded area shows the surface boundary. The location of the Inagi tornado is indicated by the solid square.

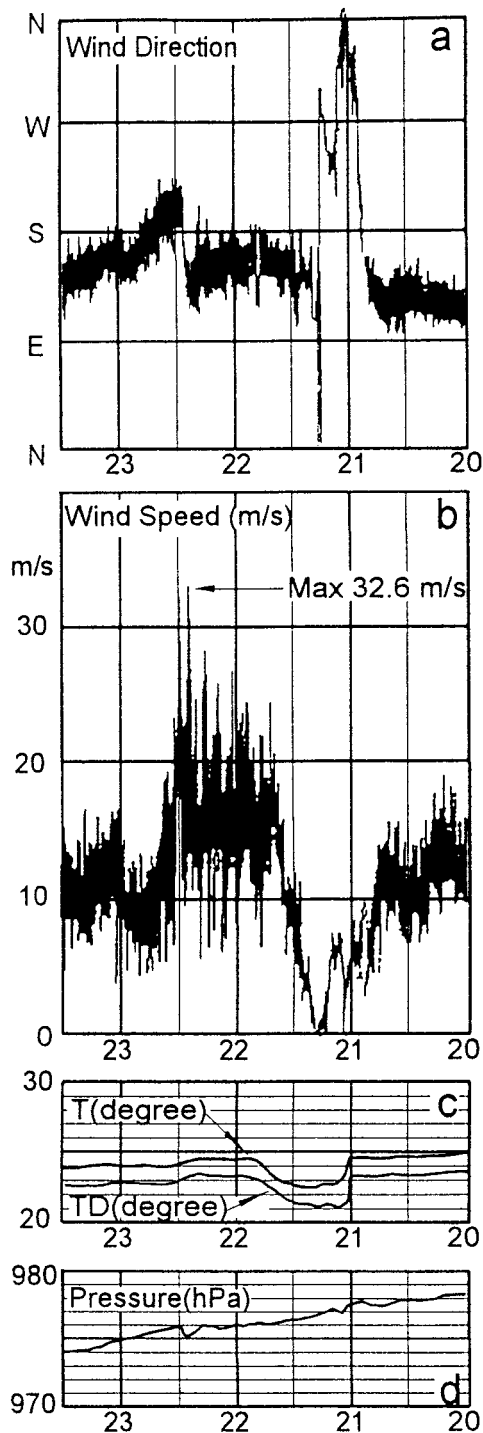


FIG. 8. Traces of (a) wind direction, (b) wind speed, (c) temperature and dewpoint temperature, and (d) surface pressure at Utsunomiya local meteorological observatory (ULMO) between 2000 and 2330 JST.

caused by outflow from storm D, which produced the Inagi tornado.

From 1800 to 2100 JST the bandlike echo cluster over the western Kanto Plain moved eastward (Figs. 4c–f), the surface boundary also drifted slowly eastward

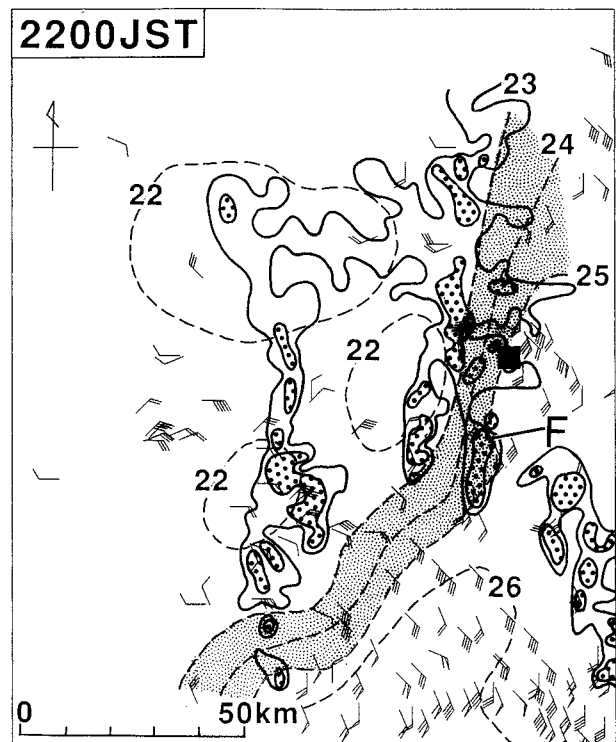


FIG. 9. Same as Fig. 7 but at 2200 JST. The location of the Mibu tornado is indicated by the solid square.

in the northern part of the Kanto Plain. In the southern part of the Plain, on the other hand, the boundary retreated westward. After 2100 JST, the boundary remained stationary, though some fluctuations, related to the passage of storms near or over the boundary, were observed.

Figure 8 shows the traces of wind direction, wind speed, temperature, dewpoint temperature, and pressure from 2000 to 2300 JST at Utsunomiya Local Meteorological Observatory (ULMO, see Fig. 2). Around 2100 JST, a sharp temperature drop of 2 K over 5 min was recorded, caused by a passage of the surface boundary toward the east. The boundary returned from the east around 2140 JST.

Figure 9 shows distributions of surface wind and temperature at 2200 JST. The boundary was located 5–10 km west of the Mibu Town (solid square in the figure), displaying an eastward protuberance near the storm F, which produced the Mibu tornado around 2215–2200 JST, like the one near storm D in Fig. 7.

Temperature gradient and vertical vorticity across the boundary are evaluated from the data at 1900 and 2200 JST. The temperature data at Chofu Airport Meteorological Observatory (CAMO in Fig. 2) and Tachikawa (about 11 km apart, not included) show that a temperature gradient across the boundary of at least $3.5 \text{ K } (10 \text{ km})^{-1}$ at 1900 JST. A similar value, about $3 \text{ K } (10 \text{ km})^{-1}$, was also observed near ULMO at 2200 JST. The vertical vorticities at 1900 and 2200 JST were estimated to be

TABLE 1. Summary of tornadoes and wind damages.

Place	Time period	F*	Path length and width (km)	Phenomenon (rotation)	House damages			Data source
					Com-pletely	Partly	In-jured	
Inagi city	1900–20	F1	5.0×0.2	Tornado (cyclonic)	2	118	0	T. Hosoda (1990, unpublished manuscript)
Shimotsuma city and Chiyakawa village	Around 2200	F0	—	Heavy winds	0	0	0	Local governments and newspaper
Mibu town	2215–20	F2	3.4×0.4	Tornado (cyclonic)	32	188	23	The authors
Azuma village	Around 0010	F1	1.0×0.03	Tornado (cyclonic)	0	10	2	The authors

* F denotes Fujita scale.

at least $4 \times 10^{-4} \text{ s}^{-1}$ [$\sim 4 \text{ m s}^{-1} (10 \text{ km})^{-1}$] in the boundary (see Figs. 7 and 9).

5. Tornadoes and storm characteristics

a. Tornadoes

Typhoon 9019 produced four tornadoes from 1350 JST on 19 to 0010 JST 20 September (see Fig. 1). All the tornadoes occurred in the northeast quadrant of the typhoon. This fact is consistent with the findings of previous statistical studies: the northeast quadrant of a hurricane (Novlan and Gray 1974; Gentry 1983) or the right-forward quadrant relative to a typhoon/hurricane motion is the preferred location of hurricane/typhoon-associated tornadoes (Fujita et al. 1972; Mitsuta 1983; McCaul 1991). Three of the tornadoes on the Kanto Plain occurred after 1900 JST (see Fig. 1). The Inagi tornado, estimated as F1 in the Fujita scale, occurred between 1900 and 1920 JST. Two F0 damage swaths produced by heavy winds (not identified as tornadoes) occurred in Chiyokawa Village around 2150 and in Shimotsuma City around 2200 JST. The most intense tornado, ranked as F2, occurred in Mibu Town between 2215 and 2200 JST. The Azuma tornado occurred around 0010 JST. Rotation in all the three tornadoes was cyclonic.

In contrast to the Inagi and the Mibu tornadoes, which occurred near/over the surface boundary, the Azuma tornado and damage-producing winds in Shimotsuma City and Chiyokawa Village (S and C in Fig. 1) occurred about 50 km and 25 km east of the boundary, respectively, and did not have relation to the boundary. Damage in Azuma, Shimotsuma, and Chiyokawa, however, was minor when compared to that caused by the Inagi and the Mibu tornadoes.

Characteristics of the three tornadoes and the two heavy winds are summarized in Table 1.

b. Supercell identification

During the night of 19 September 1990, a total of nine supercell storms were identified over the Kanto Plain by the Doppler radar. Recent studies (Weisman and Klemp 1982; Doswell et al. 1990; Doswell and

Burgess 1993) suggest that a supercell may be properly defined as a storm that contains a rotating updraft called a mesocyclone. In this paper, we adopt this definition of a supercell. However, the presence of an updraft near a vortex is difficult to identify because vertical velocity information cannot be extracted from a single Doppler radar data with lower elevation angles. Therefore, to identify a supercell, features, such as persistency, weak echo region (WER), bounded weak echo region (BWER), and/or hook echoes are used, in addition to the following mesoscale vortex identification criteria (Donaldson 1970): 1) A pair of maximum and minimum of Doppler velocities is detected on at least two adjacent elevation angles and two successive scans, 2) the angle between beam direction and a horizontal vector perpendicular to the vector pointing out the velocity maximum from the velocity minimum is less than 45° , 3) vertical vorticity is greater than $1.0 \times 10^{-2} \text{ s}^{-1}$, where the vertical vorticity was calculated by dividing the difference of the maximum and minimum Doppler velocities by their distance and multiplying by a factor of two. A vortex is assumed to be approximated by a Rankine combined vortex and its diameter is defined as a core diameter of the solid rotation, which is estimated by the distance between a Doppler velocity maxima couplet. Throughout this paper, the term “mesocyclone” (MC) will be used to denote either misocyclone or mesocyclone regardless of its diameter for simplicity (cf. Fujita 1981).

There is, however, a problem in the estimation of MC diameter and velocity difference. Brown and Lemon (1976) demonstrated that measurement of MC size and velocity maxima depend significantly upon the vortex size to the effective radar beam width. The estimated values of vertical vorticity presented in this paper will be underestimated because the diameter of MC was nearly comparable to the azimuthal resolution of the radar beam. This effect causes not only underestimation of vertical vorticity, but also a failure to detect a distant MC from the radar. Although this effect deteriorates the accuracy of the estimation, trend of the vertical vorticity of MC may be judged reliable because the movement of the MC corresponds smoothly with the effective beam width during a volume scan.

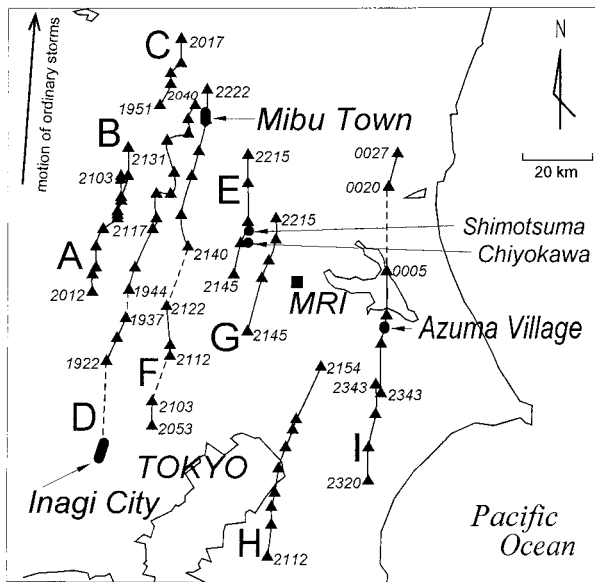


FIG. 10. Movement of mesocyclones and storms detected by the MRI Doppler radar on the night of 19 Sep 1990. The solid triangles connected by thin lines show the locations of mesocyclones. Numerals by the triangles indicate the beginning or end time of the detection of mesocyclones. Mesocyclone paths in the same storms are connected with dashed lines. Thick lines and solid circles show the location of damages by tornadoes (Inagi City, Mibu Town, and Azuma village) and heavy winds (Chiyokawa and Shimotsuma), respectively.

Figure 10 shows the path of each detected MC center within the supercells observed during a period from 1922 JST 19 September to 0100 JST 20 September. All of the supercell storms, labeled A–I, moved \sim N–NNE at average speeds of $16\text{--}19\text{ m s}^{-1}$.

Storms A, C, D, and I showed little jumps in MC paths toward the east, likely indicating cyclic generation of MC cores (e.g., Brandes 1977; Burgess et al. 1982; Johnson et al. 1987). In fact, multiple cores were detected in storm I at 2343 JST. It is noted, however, that not all the storms observed during the period were supercells (see Fig. 4). The average movement vector of ordinary storms during the period is also denoted for reference in the upper-left corner of Fig. 10, with an absolute value of 25 m s^{-1} . The movement of the supercell storms was about 30% slower than that of the ordinary storms, but in nearly the same direction as that of the ordinary storms. The movement of supercell storms showed little deviation to the right of the density-weighted mean wind below 10 km AGL (see Fig. 6). A similar feature in the storm motion was also noted by McCaul (1987) for miniature supercells associated with hurricane Danny in 1985 and by Omoto (1982) for the tornado-producing storm associated with typhoon 7912.

c. Inagi storm and Mibu storm

Storms D and F, respectively, the parent storm of the Inagi and Mibu tornadoes, displayed similar life cycles.

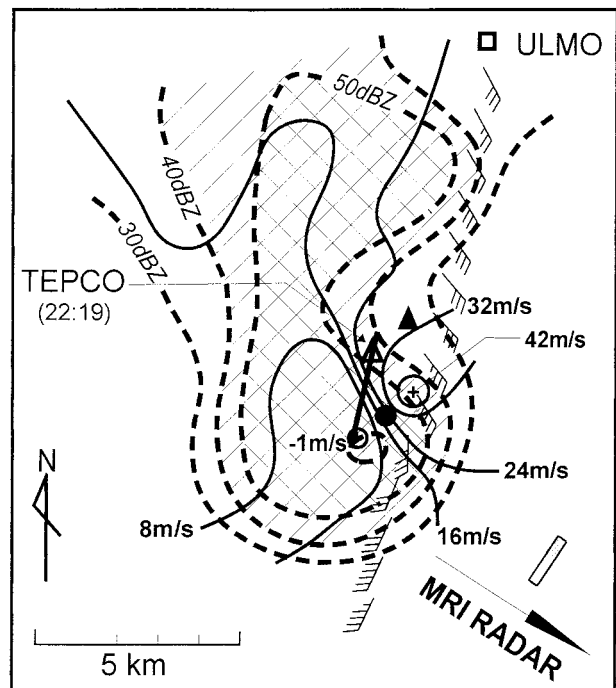


FIG. 11. PPI display of Doppler velocity and radar reflectivity with elevation angle 1.4° near Mibu town at 2216 JST. The mesocyclone center at 2216 JST is indicated by the solid circle. Contour intervals of Doppler velocity and reflectivity are 8 m s^{-1} and 10 dBZ, respectively. The Utsunomiya Local Meteorological Observatory (ULMO) is indicated by an open square. Space-to-time converted 1-min-averaged winds observed at ULMO are indicated by barbs: full barb = 5 m s^{-1} , half barb = 2.5 m s^{-1} . The tornado damage path is shown by the thick straight line and the power line of TEPCO cut by the tornado at 2219 JST is also indicated by the solid triangle. Estimated locations of the tornado and the MC center at 2219 JST is indicated by solid and dashed open triangles, respectively. The rectangle in lower right shows size of radar resolution.

Both storms were first detected near the Ohshima Island (see Figs. 4b and 4e) as isolated cells at 1645 and 1953 JST by Tokyo radar, moving north-northeastward at average speeds of 18 m s^{-1} and 17 m s^{-1} , respectively. As they moved to the north, their northern parts merged with the bandlike echo cluster over the western Kanto Plain while keeping their identities. They were tracked until 2100 and 2300 JST, respectively.

The maximum radar reflectivity cores of the storms D and F were located near their southern extents, exhibited elongated beanlike or even ribbonlike (Figs. 7, 9) shapes, and had reflectivity intensities of about 50 dBZ and 55 dBZ, respectively. The Haneda radar and the MRI Doppler radar several times identified a hook-shaped echo, a WER, and/or a BWER near at the southern end of the storms D and F. Echo top heights of both storms were approximately 10 km AGL. An MC was detected in the midlevels (2.1–4.0 km AGL) of the southeastern edge of the storm D at 1922 JST lasting until 2040 JST.

Figure 11 shows a PPI display of Doppler velocity and reflectivity fields of storm F with elevation angle

of 1.4° at 2216 JST, nearest time of the Mibu tornado. A pair of local maximum ($+42 \text{ m s}^{-1}$) and minimum (-1 m s^{-1}) of Doppler velocities is seen. The diameter of the MC was 1.5 km and the vertical vorticity $3.3 \times 10^{-2} \text{ s}^{-1}$. The reflectivity core of the storm was kidney-bean like in shape and a WER was located at the northern edge of the MC. The open triangle on the tornado path shows the tornado's location at 2219 JST, verified by damage to a TEPCO power line. The solid triangle shows an estimated location of the MC center at the same time, assuming the translational speed of 17 m s^{-1} to the north-northeast. The tornado appears to be located near the southwest edge of the MC core and was not coaxial.

One-minute averaged surface wind relative to the storm motion observed at ULMO were space-to-time converted and plotted in Fig. 11 by assuming the same translational speed and direction. These values clearly present a cyclonic circulation around the MC and the passage of a rear flank gust front (RFG). The temperature drop associated with the RFG was about 0.4 K. This RFG could not be identified in Doppler velocity fields around the time of Mibu tornado. The reason may be that Mibu town was too distant (approximately 54 km at this time) to observe the wind field near the surface due to the high beam altitude (approximately 0.66 km AGL) and the broad beamwidth.

Surface mesolows were detected in storms D and F through analysis of surface meteorological records. As storm F passed 2–3 km west of ULMO around 2222 JST, a pressure drop of 1 hPa over 10 min at 2220, a gust of 32.6 m s^{-1} , and a clockwise rotation of the wind direction were observed. This pressure drop is thought to have been caused by a mesolow associated with the MC. The diameter of the mesolow estimated from the pressure change was at least 11.8 km, assuming a translational speed of 17 m s^{-1} as the storm motion. The diameter of the mesolow at 2222 JST is about twice the diameter of the MC's core (approximately 6 km), as estimated through the Doppler velocity field and assuming a Rankine combined vortex. The difference in the estimated diameters of the mesolow and the MC may be explained by a formation of a downshear mesolow, a feature often observed in supercell storms in the United States (cf. Charba and Sasaki 1971) or an extended surface low pressure beyond the MC core region. Around 2035 JST, prior to the detection of MC in storm F, a mesolow was also observed at Yokohama Local Meteorological Observatory (YLMO, see Fig. 2) located about 80 km south-southwest of the MRI radar. That no MC was detected by the MRI radar at this time suggests that the storm was too distant and the MC too small for adequate radar resolution due to the beam-broadening effect.

Similar meteorological records were observed at the CAMO (see Fig. 4d) around 1905 JST when the storm D passed over the observatory. A sharp pressure drop of 1.5 hPa over 7 min at 1859 JST, followed by a pres-

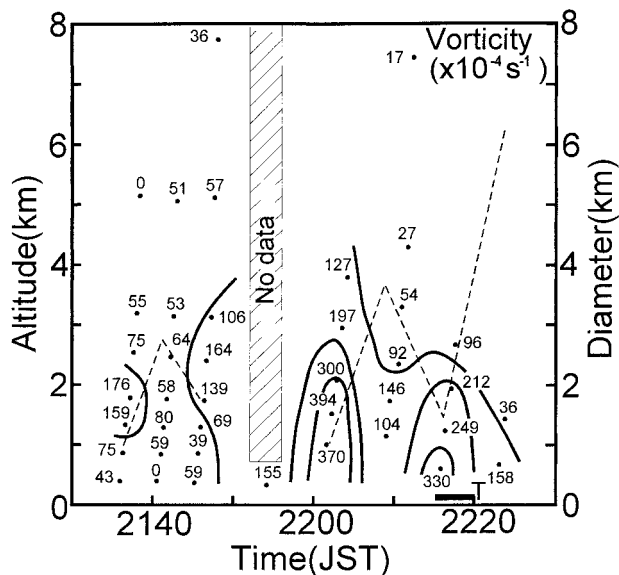


FIG. 12. The time–height cross section of vertical vorticity of the mesocyclone in the parent storm (storm F) of Mibu tornado as observed by the MRI Doppler radar. Contour interval is $5 \times 10^{-3} \text{ s}^{-1}$. Mibu tornado occurred at around 2215–2220 JST when low-level vertical vorticity reached the last maximum. The diameter of the mesocyclone at 1–2 km is shown by the dashed line. Note that PPI data at 2156 JST were taken only at the lowest angle.

sure rise of 2.3 hPa at 1906 JST, a temperature drop of about 0.5 K, anticlockwise rotation of the wind direction from 1858 to 1910 JST, and a gust of 12.3 m s^{-1} at 1906 JST were observed. These changes infer the passage of a mesolow with a RFG east of CAMO.

Figure 12 is a time-height cross section of vertical vorticity and diameters of the MC in storm D estimated from the Doppler radar data assuming a Rankine combined vortex. As mentioned in 5a, the vertical vorticity presented in the figure may be somewhat underestimated because of the beam-broadening effect (Brown and Lemon 1976). Therefore, estimated vertical vorticity can be used as a minimum bound of the true vertical vorticity.

The region with vertical vorticity greater than $1.0 \times 10^{-2} \text{ s}^{-1}$ seems always confined to the levels below 4 km AGL. It reached the first maximum of $3.9 \times 10^{-2} \text{ s}^{-1}$ at 1.6 km AGL 15 min prior to the touch down of the tornado, decreasing slightly but then again strengthening, reaching the second maximum $3.3 \times 10^{-2} \text{ s}^{-1}$ right before touch down. It is noteworthy that, immediately prior to tornadogenesis, the vorticity was largest at the lowest elevation angle (at 600 m AGL) and decreased monotonically upward. A similar intensification of low-level circulation prior to tornado touch down was often observed in typical supercell storms (JDOP staff 1979). The MC in the storm weakened by 2229 JST, shortly before the storm moved out of the detection range of the Doppler radar.

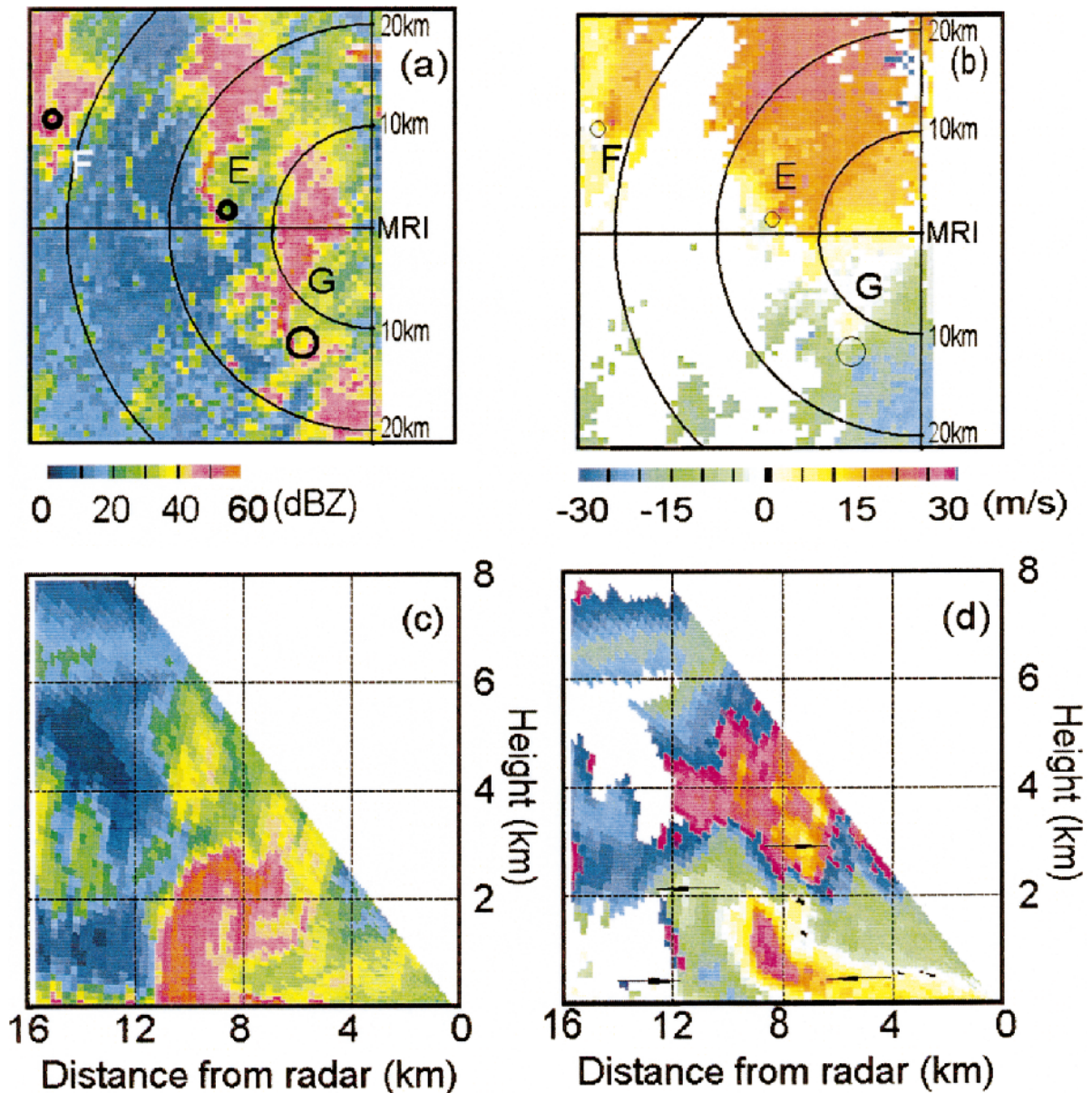


FIG. 13. The PPI display of (a) reflectivity and (b) Doppler velocity of storms E, F and G with elevation angle of 2.2° at 2146 JST. The RHI display of (c) reflectivity and (d) Doppler velocity of storm G with azimuth angle 250° at 2153 JST. The MCs are indicated by open circles in the PPI displays. Arrows in (d) indicate wind directions relative the radar deduced from the Doppler velocity field.

d. Mini supercells

Excluding storms A, B, and C, most of the supercells observed during the night of 19 September had a similar morphology to that of typical supercell storms over the Great Plains. Common features included an MC detectable by a Doppler radar, a hook-shaped echo, a WER, and/or a BWER. Most MCs were located near the southeastern edge of reflectivity cores. Storms E–I were isolated cells or cells whose southern half (core regions) were surrounded by an echo-free region throughout most of their lifetime. Cyclic MC core gen-

eration was observed in some storms; and the average lifetime was 3 h.

Figures 13a,b represent an example of a typical PPI display of radar reflectivity (Fig. 13a) and Doppler velocity (Fig. 13b) for storms E and G at 2146 JST. The MCs, indicated by open circles, are found near the southeastern edge of the strong echo region. The RHI display of the reflectivity field (Fig. 13c) derived at 2153 JST displays a vaultlike weak echo region capped by a strong echo of 3 km AGL in storm G. Corresponding Doppler velocity field (Fig. 13d) shows strong radial convergence approximately $2 \times 10^{-2} \text{ s}^{-1}$ [$\sim 40 \text{ m s}^{-1}$

TABLE 2. Comparison between typical supercells, mini supercells associated with T9019, and supercellular storms associated with Danny.

	Typical supercells over Great Plains	Mini supercells associated with T9019	Supercellular storms associated with Danny (McCaul 1987)
Morphology	Hook echo, BWER, WER	Hook echo, BWER, WER	Hook echo, wall cloud
Storm's lifetime	Several hours	3 h in average	Long life
Horizontal scale of MC	5.7 km (an average) (Burgess et al. 1979)	~1–4 km	Unknown
Vertical scale of MC	Deep (~2/3 of storm depth) (Burgess and Lemon 1990)	Lower than 5 km	Unknown
Height of initial MC	~5 km (Burgess and Lemon 1990)	~2–3 km	Unknown
Storm motion relative to mean wind	Rightward deviation and slower movement	Little rightward deviation and slower movement	Little rightward deviation and slower movement
Echo top height	Higher than 10 km	Lower than 10 km	Lower than 10 km
Hodograph	Strong deep vertical wind shear with curvature	Strong vertical wind shear with curvature below a few km AGL	Strong vertical wind shear with curvature below a few km AGL
CAPE (J kg ⁻¹)	2542 (average for Oklahoma storms; Bluestein and Jain 1985)	1 600	1984 (McCaul and Weisman 1996)
Storm relative helicity (m ² s ⁻²)	Medians are 278, 330, and 531 for F0–F1, F2–F3, and F4–F5 tornadoes (Davies-Jones et al. 1990)	310	263
BRN	10~50 (Weisman and Klemp 1982)	10	24
Ratio with tornado	About 50% (JDOP Staff 1979)	3/9	—
Multiple MC cores and cyclic core generation	Yes	Yes	Unknown

(2 km)⁻¹] below 2 km AGL and divergence between 2 and 3.5 km AGL. Figure 13d indicates a strong updraft in the vault similar to those found in typical supercell storms (e.g., Browning 1964). If we assume axisymmetry of the divergence field around the updraft and the continuity equation of fluid, this vertical distribution of convergence and divergence indicates that upward velocity increases with height below 2 km, proceeds to a maximum value, and then decreases above. These observed vertical structures are almost identical to that of a simulated supercell in hurricane Danny's environment by McCaul and Weisman (1996).

Average MC diameter ranged between 1 and 5 km, with most smaller than 4 km. Maximum vertical extent of Doppler radar-detected MCs were less than 5 km. According to Burgess et al. (1982, 1995), averaged diameters and depth of the traditional mesocyclone during mature stage are 6.0 km (midlevel) and 9.2 km, respectively. The values for the present mini supercells are almost identical to averages for WSR-88D-detected mini-supercell MCs examined by Burgess et al. (1995), but are significantly smaller than those of the MCs in typical supercells over the Great Plains. The reflectivity data (e.g., Fig. 13a) indicate that horizontal length is comparable but vertical dimension and width of these storms is much smaller than those of the typical supercell storms (e.g., schematic figures in Doswell and Burgess 1993). Some features found in the mini supercells on the night of 19 September, such as hook echo, longer life time, and smaller size compared to typical supercells, are reported by McCaul (1987) for supercellular storms that developed in Danny's environment, though, no Doppler data was available.

Several MCs passed over or close to surface meteorological stations where temperature data were available. Temperature deficit of 0.6 K at most were measured during the passage of MCs, while that of 2 K was observed across the surface boundary.

The above features are summarized in Table 2, together with features of typical supercells and supercellular storms in Danny's environment, and as schematic illustration in Fig. 14. These features demonstrate that, while their dimensions were small, the supercell storms over the Kanto Plain observed during the night of 19 September contained all the functions of typical supercells over the Great Plains.

6. Discussions

a. Spatial scale of mesocyclones in the mini supercells

The confinement of vertical vorticity to the low-level is the one of the most remarkable feature of the MCs in the presented storms. This confinement is also demonstrated in the mini supercells generated in numerical simulations under Danny's environment by McCaul (1993) and McCaul and Weisman (1996).

The reason for this confinement may be explained as follows. As shown in Fig. 6, vertical wind shear was very strong below 1 km AGL and relatively weak between 1 and 7 km AGL. As explained in many previous studies (e.g., Rotunno and Klemp 1985), vertical vorticity of a midlevel mesocyclone developed in a strong vertical wind shear is mainly generated through the tilting of ambient horizontal vorticity to vertical and the

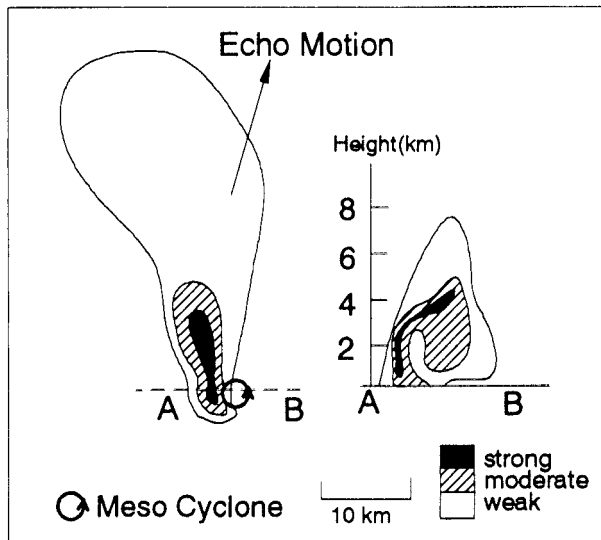


FIG. 14. A schematic of horizontal (left) and vertical (right) sections of mini supercell. Mesocyclone is located near the southeastern edge of the strong reflectivity core.

following amplification by stretching. As seen in section 5d, the vertical distribution of divergence in the mini supercells indicates strong convergence below 2 km and divergence aloft. Therefore, vertical vorticity generation by the tilting of ambient horizontal vorticity by the storm updraft would be fairly small above 2 km AGL. In the present case, generated vertical vorticity at 1–2 km AGL may have been advected upward and decreased with height above the 2 km by the stretching effect of a divergent updraft.

The small diameter of MCs in the mini supercells may be explained as follows. Since the midlevel MC is considered to be generated through tilting of horizontal vorticity in the environmental wind, the horizontal scale of the MC would nearly coincide with that of the updraft. In dry convection (i.e., Rayleigh-Benard convection), the horizontal dimension of an updraft tends to be scaled by the vertical dimension. Since the vertical scale of the mini supercell is considerably smaller than that of the typical supercell, the horizontal scales of the updraft and MC of the mini supercell are considered to be smaller than those of the typical supercell over the Great Plains.

b. Rightward deviation

As mentioned in section 5b, the movement of mini-supercell storms on the night showed little deviation to the right of the density-weighted mean wind below 10 km AGL (see Fig. 6). And mini-supercell storms and ordinary storms moved to nearly the same direction.

Rotunno and Klemp (1982) demonstrated that tilting of the horizontal vorticity of the vertically sheared basic flow by the storm updraft produces a midlevel vortex and that the vertical pressure gradient force produced

by the vortex is responsible for generating a new updraft on the right-hand side with respect to the shear vector, resulting in a rightward deviation of the storm motion. Therefore, it may be appropriate to discuss the mini-supercell storm motion in reference to the mean shear vector between surface and 1–2 km AGL, where the vertical vorticity in the MC is generated through the tilting of the ambient horizontal vorticity. In this mean, a mini-supercell storm does move rightward relative to the mean wind shear vector.

In the above paragraph, rightward deviated motion of a mini-supercell storm motion relative to the mean wind shear was explained. Then, a question may arise on the finding that the ordinary storms also moved nearly the same direction as the mini-supercell storms. Powell (1990) found that cells in the outer rainbands of hurricane Floyd (1981) moved down the band, and the rainbands oriented along the density-weighted mean wind speed of the 0.2–6-km layer. In the present case, direction of the ordinary storms motion and of the density-weighted mean wind of the layer were the almost same. Therefore, this similarity in the storms' motion between mini supercells and ordinary cells on this night is likely to be a coincidence.

c. Evaluation of vorticities in the surface boundary

As noted in section 5a, two of the stronger tornadoes, the Inagi and the Mibu, occurred when the storms were moving along the surface boundary. This suggests the possible contribution to the storms development of stretching of the preexisting vertical vorticity and the baroclinically generated horizontal vorticity.

First, the possibility of preexisting vertical vorticity amplification in an updraft is examined. The vertical vorticity equation for an inviscid incompressible homogeneous fluid is written as follows:

$$\frac{d\zeta}{dt} = \boldsymbol{\omega}_h \cdot \nabla_h w + \zeta \frac{\partial w}{\partial z}, \quad (1)$$

where ζ is the vertical vorticity, d/dt is the time derivative following the fluid parcel, $\boldsymbol{\omega}_h$ is the horizontal component of vorticity vector $\boldsymbol{\omega}$, ∇_h is the horizontal derivative vector, and w is the vertical component of the velocity vector (u, v, w). The first term on the right-hand side of Eq. (1) is the tilting term. The second term on the right-hand side is the stretching term.

After Klemp and Rotunno (1983), change over time of the vertical vorticity in an updraft with a constant convergence (denoted by w_z) and a constant tilting term (denoted by T) is evaluated. Under this assumption, one can easily integrate Eq. (1) to obtain (Klemp and Rotunno 1983),

$$\zeta(t) = \frac{T}{w_z} [e^{w_z(t-t_0)} - 1] + \zeta_0 e^{w_z(t-t_0)}, \quad (2)$$

where t_0 is the beginning time of the integration and ζ_0

is the vertical vorticity at $t = t_0$. As mentioned in section 4b, vertical vorticity in the surface boundary is on the order of $4 \times 10^{-4} \text{ s}^{-1}$. Doppler radar observation (see Fig. 13d) found a strong radial convergence reaching on the order of $1 \times 10^{-2} \text{ s}^{-1}$. If this value is used as the w_z in Eq. (2), it takes 320 s for the vertical vorticity to be amplified to $1 \times 10^{-2} \text{ s}^{-1}$ solely by the convergent stretching. Evaluated vertical vorticity of the order of 10^{-2} s^{-1} seems still insufficient to explain the rapid amplification of low-level vertical vorticity before the tornado. However, these values are not so small as to be neglected. There is a possibility that additional vorticity generated by the above mechanism makes a contribution to the amplification of supercell development and resultant tornadogenesis as in a nonsupercell tornado development mechanism (Wakimoto and Wilson 1989).

Second, horizontal vorticity generated by baroclinic effect is roughly evaluated with a calculation after Klemp and Rotunno (1983). The estimated value is approximately a quarter of averaged environmental horizontal vorticity on the order of $2 \times 10^{-3} \text{ s}^{-1}$ between the surface and 1 km (Fig. 6). It indicates that streamwise horizontal vorticity generated in the baroclinic zone along the forward flank gust front is less important in the case of our mini-supercell storms than in the case of typical supercell storms, even though this estimation may have errors because the data available were insufficient to describe temperature field in the storms.

7. Summary and conclusions

On the night of 19 September 1990, nine mini supercells were observed over the Kanto Plain in the northeast quadrant of Typhoon 9019. The supercell environment was characterized by a modest CAPE (about 1600 J kg^{-1}) and a strong low-level veering wind shear. The mini supercells had several features similar to the Great Plains supercells, including an indication of cyclic mesocyclone evolution. However, single Doppler radar and conventional radar observations revealed that MCs in the mini supercells had smaller diameters ($\sim 1\text{--}5 \text{ km}$), and the extent of vertical vorticity was smaller (below 5 km AGL). These features are similar to mini supercells observed in the United States.

Three mini supercells out of nine spawned a tornado. Two of the tornadoes occurred near the preexisting surface boundary. It was suggested that the stretching of the vertical vorticity in the surface boundary likely contributed to the amplification of the vertical vorticity of the MCs in the low-level to the marginal value over which a tornadogenesis is possible.

Recently, the authors' group identified several supercell storms that produced tornado in the Kanto Plain associated with extratropical cyclones using Doppler radar data (e.g., Suzuki et al. 1997). Most of these supercells were small and shallow storms. In addition to the Doppler radar-detected mini supercells in Japan, a statistical study was conducted by the authors' group in

the Okinawa area on the relationship between atmospheric vortices and environmental indices (Suzuki, Niino and Cooperative Research Group of Okinawa Observatory 94–95 1998). This study, though limited to the Okinawa area, revealed that 33% and 67% of tornadoes occurred in environments with high storm relative helicity ($>150 \text{ m}^2 \text{ s}^{-2}$) and low BRN (<50), respectively. These findings together with the present paper suggest that a significant fraction of tornado-producing storms in Japan are mini supercells. The diminutive dimensions of the mini supercell and the limited availability of reliable Doppler radar analyses hinder the understanding of the dynamics of mini supercell and associated tornadoes, as mentioned in the earlier section. Further observational and numerical studies on the mini supercells are needed for the more complete understanding of the mini supercells and related tornadoes.

Acknowledgments. The authors wish to thank to the metropolitan office of Tokyo, the prefectural offices of Tochigi, Saitama, Kanagawa, Ibaraki, and Chiba, the city offices of Utsunomiya, Yokohama, Kawasaki, Fujisawa, Sagami-hara, and Yokosuka, the town office of Mibu, Tokyo electric power company, and JMA for providing meteorological data. Thanks are extended to Mrs. K. Yoshiye and Miss Ohyoshi for preparing the figures. This research was partly supported by the Grant-in-Aid for Scientific Research (No. 09440166) of the Japanese Ministry of Education, Science, Sports and Culture.

REFERENCES

- Asai, T., and K. Takahashi, 1981: On the quasi-stationary rain band observed in the Kanto District on 9 September 1976. *J. Natural Disaster Sci.*, **4**, 33–44.
- Bluestein, H. B., and M. H. Jain, 1985: Formation of mesoscale lines of precipitation: Severe squall lines in Oklahoma during the spring. *Mon. Wea. Rev.*, **115**, 2719–2727.
- Brandes, E. A., 1977: Gust front evolution and tornadogenesis as viewed by Doppler radar. *J. Appl. Meteor.*, **16**, 333–338.
- Brown, R. A., and L. R. Lemon, 1976: Single Doppler radar vortex recognition. Part II: Tornadic vortex signatures. Preprints, *17th Radar Meteorology Conf.*, Seattle, WA, Amer. Meteor. Soc., 104–109.
- Browning, K. A., 1964: Airflow and precipitation trajectories within severe local storms which travel to the right of the winds. *J. Atmos. Sci.*, **21**, 634–668.
- Burgess, D. W., and L. R. Lemon, 1990: Severe thunderstorm detection by radar. *Radar in Meteorology*, D. Atlas, Ed., Amer. Meteor. Soc., 619–647.
- , V. T. Wood, and R. A. Brown, 1982: Mesocyclone evolution statistics. Preprints, *12th Conf. on Severe Local Storms*, San Antonio, TX, Amer. Meteor. Soc., 422–424.
- , R. L. Lee, S. S. Parker, S. J. Keighton, and D. L. Floyd, 1995: A study of mini supercells observed by WSR-88D radars. Preprints, *27th Conf. on Radar Meteor.*, Vail, CO, Amer. Meteor. Soc., 4–6.
- Charba, J., and Y. Sasaki, 1971: Structure and movement of the severe thunderstorms of 3 April 1964 as revealed from radar and mesonetwork data analysis. *J. Meteor. Soc. Japan*, **49**, 191–214.
- Davies, J. M., 1993: Small tornadic supercells in the central plains.

- Preprints, *17th Conf. on Severe Local Storms*, St. Louis, MO, Amer. Meteor. Soc., 305–309.
- Davies-Jones, R. P., 1993: Helicity trends in tornado outbreaks. Preprints, *17th Conf. on Severe Local Storms*, St. Louis, MO, Amer. Meteor. Soc., 56–60.
- , D. Burgess, and M. Foster, 1990: Test of helicity as a tornado forecast parameter. Preprints, *16th Conf. on Severe Local Storms*, Kananaskis Park, AB, Canada, Amer. Meteor. Soc., 588–592.
- Donaldson, R. J., Jr., 1970: Vortex signature recognition by a Doppler radar. *J. Appl. Meteor.*, **9**, 661–670.
- Doswell, C. A., III, and D. W. Burgess, 1993: *The Tornado: Its Structure, Dynamics, Prediction, and Hazards*. *Geograph. Monogr.*, No. 79, Amer. Geophys. Union, 161–172.
- , A. R. Moller, and R. Przybylinski, 1990: A unified set of conceptual models for variations on the supercell theme. Preprints, *16th Conf. on Severe Local Storms*, Kananaskis Park, AB, Canada, Amer. Meteor. Soc., 334–339.
- Fujita, T. T., 1981: Tornadoes and downbursts in the context of generalized planetary scales. *J. Atmos. Sci.*, **38**, 1511–1533.
- , K. Watanabe, K. Tsuchiya, and M. Shimada, 1972: Typhoon-associated tornadoes in Japan and new evidence of suction vortices in a tornado near Tokyo. *J. Meteor. Soc. Japan*, **50**, 431–453.
- Gentry, R. C., 1983: Genesis of tornadoes associated with hurricanes. *Mon. Wea. Rev.*, **111**, 1793–1805.
- Guerrero, H., and W. Read, 1993: Operational use of the WSR-88D during the November 21, 1992 southeast Texas tornado outbreak. Preprints, *17th Conf. on Severe Local Storms*, St. Louis, MO, Amer. Meteor. Soc., 399–402.
- JDOP staff, 1979: Final report of the Joint Doppler Operational Project. NOAA Tech. Memo. ERL NSSL-86, National Severe Storms Laboratory, Norman, Oklahoma, 84 pp. [NTIS PB80-107 188/AS; Available from National Technical Information Service, 5285 Port Royal Rd., Springfield, VA 22161.]
- Johnson, K. W., P. S. Ray, B. C. Johnson, and R. P. Davies-Jones, 1987: Observations related to the rotational dynamics of the 20 May 1977 tornadic storms. *Mon. Wea. Rev.*, **115**, 2463–2478.
- Kawamura, T., 1970: Surface wind systems over central Japan in the warm season—With special reference to the southwesterly flow pattern (in Japanese with English abstract). *Geo. Rev. Japan*, **43**, 203–210.
- Kemp, J. B., and R. Rotunno, 1983: A study of the tornadic region within a supercell thunderstorm. *J. Atmos. Sci.*, **40**, 359–377.
- Markowski, P. M., J. M. Straka, E. N. Rasmussen, and D. O. Branchard, 1998: Variability of storm-relative helicity during VORTEX. *Mon. Wea. Rev.*, **26**, 2959–2971.
- McCaul, E. W., Jr., 1987: Observations of the hurricane “Danny” tornado outbreak of 16 August 1985. *Mon. Wea. Rev.*, **115**, 1206–1223.
- , 1991: Buoyancy and shear characteristics of hurricane-tornado environments. *Mon. Wea. Rev.*, **119**, 1954–1978.
- , 1993: Hurricane spawned tornadic storms. *The Tornado: Its Structure, Dynamics, Prediction, and Hazards*, *Geograph. Monogr.*, No. 79, Amer. Geophys. Union, 119–142.
- , and M. L. Weisman, 1996: Simulations of shallow supercell storms in landfalling hurricane environments. *Mon. Wea. Rev.*, **124**, 408–429.
- Mitsuta, Y., Ed., 1983: Studies on wind disasters caused by tatsumaki (tornadoes and waterspouts) and severe local storms in Japan (in Japanese with English abstract). Final Report of the Special Research Project for Natural Disaster Sponsored by the Ministry of Education, 124 pp.
- Niino, H., O. Suzuki, H. Nirasawa, T. Fujitani, H. Ohno, I. Takayabu, N. Kinoshita, and Y. Ogura, 1993: Tornadoes in Chiba prefecture on 11 December 1990. *Mon. Wea. Rev.*, **121**, 3001–3018.
- Novlan, D. J., and W. M. Gray, 1974: Hurricane-spawned tornadoes. *Mon. Wea. Rev.*, **102**, 476–488.
- Omoto, Y., 1982: On “tatsumaki” (tornadoes) associated with typhoons (in Japanese). *Tenki*, **29**, 967–980.
- Powell, M., 1990: Boundary layer structure and dynamics in outer hurricane rainbands. Part I: Mesoscale rainfall and kinematic structure. *Mon. Wea. Rev.*, **118**, 891–917.
- Rotunno, R., and J. B. Kemp, 1982: The influence of the shear-induced pressure gradient on thunderstorm motion. *Mon. Wea. Rev.*, **110**, 136–151.
- , and —, 1985: On the rotation and propagation of simulated supercell thunderstorms. *J. Atmos. Sci.*, **42**, 271–292.
- Saito, A., 1992: Mesoscale analysis of typhoon-associated tornado outbreaks in Kyushu Island on 13 October 1980. *J. Meteor. Soc. Japan*, **70**, 43–55.
- Sekiguchi, T., T. Yoshidama, and M. Taniharu, 1964: Geographic distribution of hourly typhoon rainfall and radar echoes in the Kanto Plain, eastern Japan—Formation of orographic rain-bands (in Japanese with English abstract). *Geo. Rev. Japan*, **37**, 55–62.
- Snell, W. L., and E. W. McCaul, 1993: Doppler signatures of tornadoes spawned by hurricane Andrew near Montgomery, Alabama. Preprints, *26th Conf. on Radar Meteorology*, Norman, OK, Amer. Meteor. Soc., 80–82.
- Suzuki, O., H. Niino, and Cooperative Research Group of Okinawa Observatory 94–95, 1998: A statistical study on tornadoes, waterspouts, and funnels aloft in Okinawa prefecture in Japan. Preprints, *19th Conf. on Severe Local Storms*, Minneapolis, MN, Amer. Meteor. Soc., 105–107.
- , Y. Tanaka, K. Kusunoki, and Y. Makihara, 1997: Supercell evolution observed with a high resolution Doppler radar. Preprints, *28th Conf. on Radar Meteorology*, Austin, TX, Amer. Meteor. Soc., 538–539.
- Wakimoto, R. M., and J. W. Wilson, 1989: Non-supercell tornadoes. *Mon. Wea. Rev.*, **117**, 1113–1140.
- Weisman, M. L., and J. B. Klemp, 1982: The dependence of numerically simulated convective storms on vertical wind shear and buoyancy. *Mon. Wea. Rev.*, **110**, 504–520.